Nanocomposite Prepared from *In Situ* Grafting of Polypyrrole to Aminobenzoyl-Functionalized Multiwalled Carbon Nanotube and Its Electrochemical Properties

IN-YUP JEON,[1] HYUN-JUNG CHOI,[1] LOON-SENG TAN,[2] JONG-BEOM BAEK[1]

[1]Interdisciplinary School of Green Energy/Institute of Advanced Materials & Devices, Ulsan National Institute of Science and Technology (UNIST), 100, Banyeon, Ulsan 689-798, South Korea

[2]Nanostructured and Biological Materials Branch, Materials and Manufacturing Directorate, U.S. Air Force Research Laboratory, AFRL/RXBN, Wright-Patterson AFB, Ohio 45433

ABSTRACT: We reported the functionalization of multiwalled carbon nanotube (MWCNT) with 4-aminobenzoic acid by a "direct" Friedel–Crafts acylation reaction in a mild polyphosphoric acid (PPA)/phosphorous pentoxide (P_2O_5) medium. The resulting 4-aminobenzoyl-functionalized MWCNT (AF-MWCNT) was used as a platform for the grafting of polypyrrole (PPy) in ammonium persulfate (APS)/aqueous hydrochloric acid solution to produce PPy-grafted MWCNT (PPy-*g*-MWCNT) composite. After dedoping with alkaline treatment, PPy-*g*-MWCNT displayed 20 times higher electrical conductivity than that of PPy. The current density and cycle stability of PPy-*g*-MWCNT composite were also remarkably improved compared with those of PPy homopolymer, suggesting that an efficient electron transfer between PPy and MWCNT was possible through covalent links. In addition, PPy-*g*-MWCNT displayed high electrocatalytic activity for oxygen reduction reaction (ORR). © 2011 Wiley Periodicals, Inc. J Polym Sci Part A: Polym Chem 49: 2529–2537, 2011

KEYWORDS: conducting polymers; electrochemistry; grafting; multiwalled carbon nanotube; nanocomposites; polypyrrole

INTRODUCTION Conducting polymers such as polypyrrole (PPy), polyaniline (PANi), poly(*p*-phenylene vinylene) (PPV), and polythiophene (PT) and their derivatives are attractive materials for the electrochemical devices.[1–3] The conducting polymers have many advantages such as low cost, easy processing, and light weight over metallic conductors. Similar to PANi, PPy has an important commercialization potential due to its good conductivity, easy synthesis, and long-term environmental stability.[3–5] Therefore, PPy can offer a variety of potential applications such as electrically conducting composites,[6] actuators,[7,8] supercapacitors,[9] and electrochromic[10] and photovoltaic[11] applications. Although the doping level of conducting polymers can be readily controlled by an acid-doping/base-dedoping cycles,[12] they generally have poor mechanical properties. Thus, they were copolymerized or blended with ductile but insulating polymers to improve mechanical properties. In this case, the doping level of copolymers or polymer blends is limited because of the portion of insulating polymers,[13] resulting in poor conductivity of these systems.[14] To improve the mechanical properties as well as electrical conductivity at the same time, hybridization of conductive carbon nanomaterials (CNMs) and conducting polymers is worth to exploit.

CNMs such as carbon nanotubes (CNTs), carbon nanofibers (CNFs), and graphene have been received much interest for their uses in fabricating a new class of advanced materials because of their unique structural, mechanical, and electrical properties.[15,16] As expected to show high stability, good electrical and mechanical properties, the incorporation of CNTs into polymer matrices has been intensively studied to improve not only the mechanical but also the electrical properties of the polymers.[17–20] The conducting polymer-based CNT composites including poly(phenylene sulfide) (PPS)/multiwalled carbon nanotube (MWCNT),[21] PANi/MWCNT,[22] and PPV/CNT[23] have displayed improved synergistic properties emerging from the contributions of each component.[24] To obtain maximum enhanced properties, homogeneous dispersion of CNT into the supporting polymer matrices and interfacial interactions between them should be addressed first. Hence, harsh chemical treatments in strong acids such as sulfuric acid, nitric acid, or their mixtures with/without sonication have been commonly applied.[25,26] However, these treatments often result in various types of structural damage to the CNT framework, which involve sidewall opening, breaking, chemical oxidation, and turning into amorphous carbon.[27–30] Such treatments help the dispersion of CNTs due to entropy gains from size reduction and enthalpy gains from creation of oxygenated surface moieties. Unfortunately, however, these types of damage on CNTs cannot preserve

Report Documentation Page

1. REPORT DATE **14 APR 2011**	2. REPORT TYPE	3. DATES COVERED **00-00-2011 to 00-00-2011**

4. TITLE AND SUBTITLE	5a. CONTRACT NUMBER
Nanocomposite Prepared from In Situ Grafting of Polypyrrole to Aminobenzoyl-Functionalized Multiwalled Carbon Nanotube and Its Electrochemical Properties	5b. GRANT NUMBER
	5c. PROGRAM ELEMENT NUMBER
6. AUTHOR(S)	5d. PROJECT NUMBER
	5e. TASK NUMBER
	5f. WORK UNIT NUMBER

7. PERFORMING ORGANIZATION NAME(S) AND ADDRESS(ES) **Ulsan National Institute of Science and Technology (UNIST),Interdisciplinary School of Green Energy & Inst of Advanced Materials & Devices,100, Banyeon,Ulsan 689-798, South Korea,**	8. PERFORMING ORGANIZATION REPORT NUMBER

9. SPONSORING/MONITORING AGENCY NAME(S) AND ADDRESS(ES)	10. SPONSOR/MONITOR'S ACRONYM(S)
	11. SPONSOR/MONITOR'S REPORT NUMBER(S)

12. DISTRIBUTION/AVAILABILITY STATEMENT
Approved for public release; distribution unlimited

13. SUPPLEMENTARY NOTES

14. ABSTRACT
We reported the functionalization of multiwalled carbon nanotube (MWCNT) with 4-aminobenzoic acid by a ??direct?? Friedel?Crafts acylation reaction in a mild polyphosphoric acid (PPA)/phosphorous pentoxide (P_2O_5) medium. The resulting 4- aminobenzoyl-functionalized MWCNT (AF-MWCNT) was used as a platform for the grafting of polypyrrole (PPy) in ammonium persulfate (APS)/aqueous hydrochloric acid solution to produce PPy-grafted MWCNT (PPy-g-MWCNT) composite. After dedoping with alkaline treatment, PPy-g-MWCNT displayed 20 times higher electrical conductivity than that of PPy. The current density and cycle stability of PPy-g-MWCNT composite were also remarkably improved compared with those of PPy homopolymer, suggesting that an efficient electron transfer between PPy and MWCNT was possible through covalent links. In addition, PPy-g-MWCNT displayed high electrocatalytic activity for oxygen reduction reaction (ORR).

15. SUBJECT TERMS

16. SECURITY CLASSIFICATION OF:			17. LIMITATION OF ABSTRACT	18. NUMBER OF PAGES	19a. NAME OF RESPONSIBLE PERSON
a. REPORT **unclassified**	b. ABSTRACT **unclassified**	c. THIS PAGE **unclassified**	**Same as Report (SAR)**	**9**	

their original, outstanding electrical, thermal, and physical properties.[31]

In this regard, we have developed the less and/or nondestructive chemical modification of various CNMs by "direct" Friedel–Crafts acylation reaction in a mild polyphosphoric acid (PPA)/ phosphorous pentoxide (P_2O_5) medium.[32,33] To tackle the problems on dispersion of CNTs and interfacial adhesion between CNTs and polymer matrices, the covalent grafting of conducting polymers onto the surface of CNTs can be a great challenge to achieve maximally enhanced properties. Thus, the *in situ* grafting of PPy onto the previously 4-aminobenzoyl-functionalized (grafting sites) MWCNTs (AF-MWCNTs) was conducted to produce PPy-grafted MWCNT (PPy-*g*-MWCNT). The PPy-*g*-MWCNT composite was expected to display improved electrical conductivity and electrocatalytic activity compared with PPy homopolymer without conventional doping. Furthermore, nitrogen-containing carbon-based materials have displayed outstanding catalytic activity for oxygen reduction reaction (ORR).[34,35] Thus, PPy-*g*-MWCNT would be a good precursor for ORR catalyst.

EXPERIMENTAL

Materials

All reagents and solvents were purchased from Aldrich Chemical and Lancaster Synthesis, and used as received, unless otherwise specified. MWCNT (CVD MWCNT 95 with diameter of ~20 nm and length of 10–50 μm) was obtained from Hanhwa Nanotech, (Seoul, Korea).[36]

Instrumentation

Infrared (IR) spectra were recorded on a Jasco FT-IR 480 Plus spectrophotometer. Solid samples were imbedded in KBr disks. Elemental analyses (EA) were performed with a CE Instruments EA1110. Thermogravimetric analysis (TGA) was conducted in nitrogen and air atmospheres with a heating rate of 10 °C/min using a Perkin–Elmer TGA 7. The field emission scanning electron microscopy (FE-SEM) used in this work was LEO 1530FE. The field emission transmission electron microscope (FE-TEM) used in this work was a FEI Tecnai G2 F30 S-Twin. The surface area was measured by nitrogen adsorption–desorption isotherms using the Brunauer–Emmett–Teller (BET) method (Micromeritics ASAP 2504N). Wide-angle X-ray diffraction (WAXD) powder patterns were recorded with a Rigaku RU-200 diffractometer using Ni-filtered Cu Kα radiation (40 kV, 100 mA, λ = 0.15418 nm). UV–vis spectra were obtained on a Varian Cary 5000 UV–vis spectrometer. Stock solutions were prepared by dissolving 10 mg of each sample in 1 L of *m*-cresol. Photoluminescence measurements were performed with a Varian Cary Eclipse Fluorescence spectrometer. The excitation wavelength was that of the UV absorption maximum of each sample. Cyclic voltammetry (CV) experiments were performed with a 1470E Cell Test System (Solartron Analytical, UK). The three-electrode system consisted of a glassy carbon (GC) electrode as the working electrode, an Ag/AgCl (sat. KCl) as the reference electrode, and platinum gauze as the counter electrode. All potential values are reported versus Ag/AgCl.

The resistance of samples was measured by four-point probe method using Advanced Instrument Technology (AIT) CMT-SR1000N with Jandel Engineering probe at room temperature. The conductivity values were the average values of 10 measurements each.

Functionalization of MWCNT (AF-MWCNT)

As described in our previous reports,[37,38] the functionalization of MWCNTs with 4-aminobenzoic acid was carried out in a PPA/P_2O_5 medium at 130 °C for 72 h. The final product was sequentially Soxhlet extracted overnight with distilled water and methanol, and finally freeze-dried for 48 h to afford AF-MWCNT.

Polymerization of PPy

Pyrrole (10.0 g, 149 mmol) and 1 M aqueous HCl (120 mL) were placed into a 250-mL-three-necked, round-bottomed flask equipped with a magnetic stirrer, a reflux condenser, and a nitrogen inlet. Eighty milliliters of 1.0 M aqueous HCl solution containing 40.0 g (175 mmol) ammonium persulfate (APS) was added dropwise into the suspension with constant mechanical stirring, while maintaining the reaction temperature at 0–5 °C for 1 h. The reaction mixture was stirred for an additional 6 h at that temperature. The resulting dark black precipitate that formed was collected by filtration, washed with 1 M aqueous HCl and methanol, and then finally freeze-dried under reduced pressure (0.05 mmHg) for 48 h to give 8.51 g (86.9% yield) of dark black powder (PPy).

Synthesis of PPy-*g*-MWCNT Composite

In the same set-up for the synthesis of PPy, AF-MWCNT (1.0 g), pyrrole (9.0 g, 134 mmol), and 1 M aqueous HCl (120 mL) were placed. Eighty milliliters of 1.0 M aqueous HCl solution containing 40.0 g (175 mmol) APS was added dropwise into the suspension, while maintaining the reaction temperature at 0–5 °C for 1 h. The rest of the reaction conditions and work-up procedure were the same as the synthesis of PPy to give 7.89 g (78% yield) of dark wine-red powder (PPy-*g*-MWCNT).

Dedoping of PPy and PPy-*g*-MWCNT

As-prepared PPy and PPy-*g*-MWCNT are doped with HCl. They could be dedoped by immersion into excess of 1 M aqueous ammonium hydroxide at room temperature for 24 h. They were collected by filtration, Soxhlet extracted with distilled water, and finally freeze-dried under reduced pressure (0.05 mmHg) for 48 h to give dedoped PPy and PPy-*g*-MWCNT.

Electrochemical Properties

Cyclic voltammetry was carried out using a VersaSTAT3 AMETEK model (Princeton Applied Research, TN) potentiostat/galvanostat using a standard three-electrode electrochemical cell, which consisted of the functionalized sample/GC as the working electrode, an Ag/AgCl as the reference electrode, and platinum gauze as the counter electrode. Experiments were carried out at room temperature in 0.1 M aqueous KOH solution as the electrolyte. All potentials are reported relative to an Ag/AgCl (sat. KCl) reference electrode
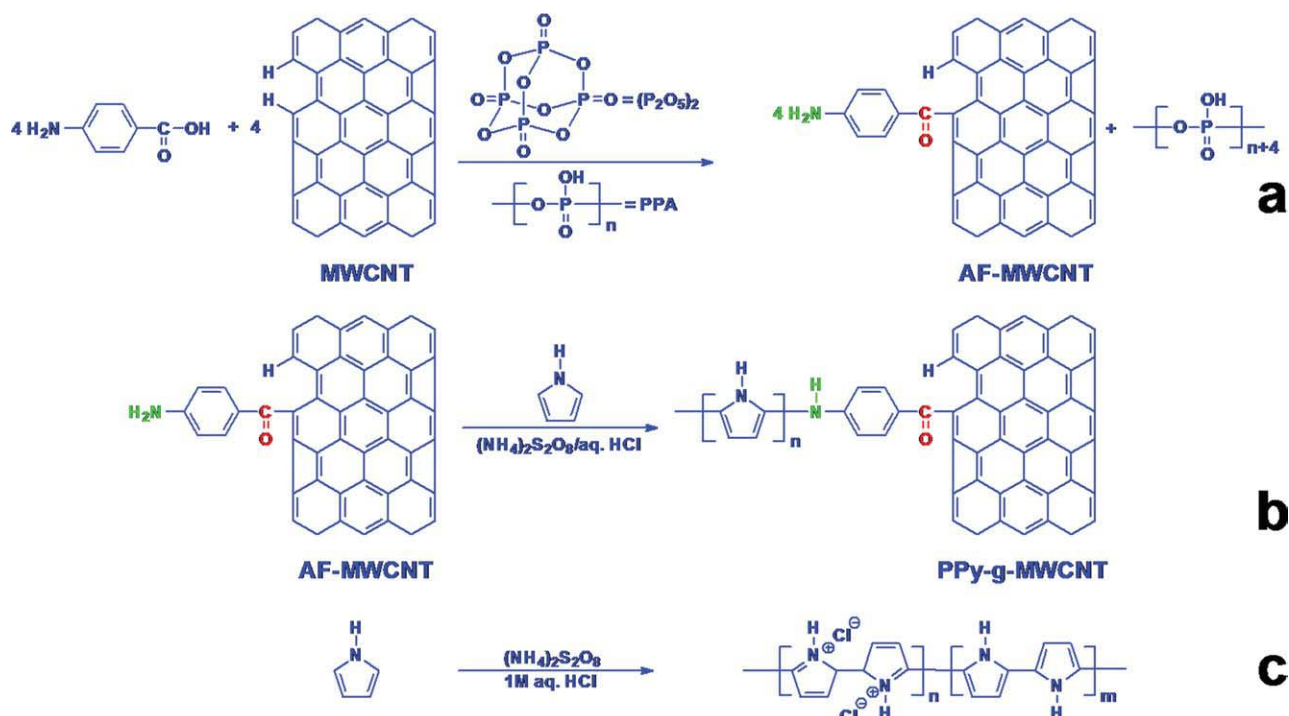
FIGURE 1 (a) Functionalization of MWCNT with 4-aminobenzoic acid in polyphosphoric acid (PPA)/phosphorous pentoxide (P_2O_5) to produce 4-aminobenzoyl-functionalized MWCNT (AF-MWCNT); (b) grafting of polypyrrole (PPy) onto the surface of AF-MWCNT in ammonium persulfate (APS)/1 M aqueous hydrochloric acid (HCl); (c) polymerization of PPy in APS/1 M aqueous HCl. [Color figure can be viewed in the online issue, which is available at wileyonlinelibrary.com.]

recorded at a scan rate of 10 mV/s. The electrocatalytic activity for ORR was also evaluated by dipping the sample/GC electrodes in an oxygen-saturated aqueous KOH (0.1 M) and H_2SO_4 electrolyte solutions with a scan rate of 10 mV/s. The procedure of the GC electrode pretreatment is described as follows: before use, the working electrode was polished with alumina slurry to obtain a mirror-like surface and then washed with deionized (DI) water and allowed to dry. The sample (1 mg) was dispersed in 0.09 mL m-cresol by brief sonication (5 min). Nafion (5%) in EtOH/water (v/v = 1:9) mixture solution (0.01 mL) was added into the sample mixtures and applied additional brief sonication (5 min). The sample suspension (10 μL) was pipetted on the GC electrode surface, followed by drying at 50 °C under reduced pressure (0.05 mmHg).

RESULTS AND DISCUSSION

To maximize the efficiency of CNTs as reinforcing and conducting additives, the effective aspect ratio and interfacial adhesion have to be achieved first. The aspect ratio is mainly determined by the degree of dispersion[39] and the interfacial adhesion is dependent on chemical affinity between CNTs and supporting matrices.[40] Hence, less and/or nondestructive chemical modification of CNTs could be the best option for resolving these issues concurrently. The nondestructive functionalization of MWCNTs was carried with 4-aminobenzoic acid in a PPA/P_2O_5 medium at 130 °C [Fig. 1(a)].[33,36] The detailed mechanism for the functionalization through a "direct" Friedel–Crafts acylation reaction involves carbonium ion ($-C^+$=O; Supporting Information Fig. S1). Water as a

byproduct, which is generated during the reaction between PPA and 4-aminobenzoic acid, is attacked by P_2O_5 converting into PPA. As a result, the reverse reaction is prevented by increasing molecular weight of PPA and the generated carbonium ion is nowhere to react with but to attack sp^2C—H present at the defects on the outer surface of MWCNTs. On the basis of characterization results from Fourier transform infrared (FTIR; Supporting Information Fig. S2a), TGA (Supporting Information Fig. S2b), SEM (Supporting Information Fig. S2c), and TEM (Supporting Information Fig. S2d), the surface of resultant AF-MWCNT was decorated well by 4-aminobenzoyl moieties, which could be the anchoring sites for the covalent attachment of PPy. Thus, the PPy was grafted onto the surface of AF-MWCNT by chemical oxidation polymerization of pyrrole in APS/1 M aqueous HCl at 0–5 °C to produce PPy-grafted MWCNT (PPy-g-MWCNT) [Fig. 1(b)]. For comparison, PPy was synthesized in the same reaction and work-up conditions as for PPy-g-MWCNT [Fig. 1(c)].

The FTIR spectrum of PPy shows the characteristic bands attributable to the C—H out-of-plane deformation vibration at 941 cm^{-1}, the C—H in-plane deformation vibration at 1041 cm^{-1}, the C—N stretching vibration at 1307 cm^{-1}, and the ring-stretching mode of pyrrole ring at 1579 cm^{-1} [Fig. 2(a)]. All characteristic peaks from PPy are clearly shown in the FTIR spectrum of PPy-g-MWCNT with some shift [Fig. 2(a)]. The existence of the C=O peaks from the spectrum of the PPy-g-MWCNT should be one of the evident proofs that AF-MWCNT and PPy are covalently bonded because they are the linking groups between them. However, the relative
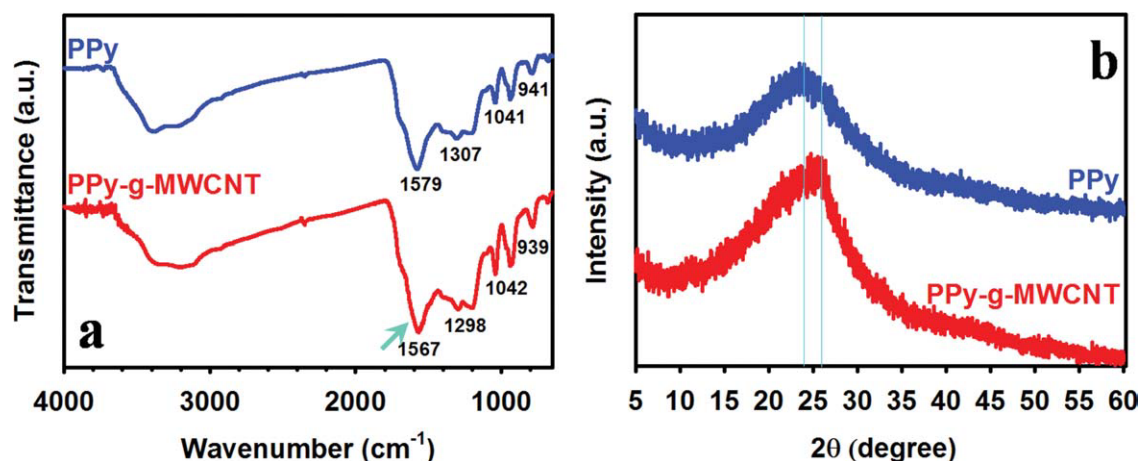
FIGURE 2 (a) FTIR (KBr pellet) spectra of PPy and PPy-*g*-MWCNT; (b) XRD powder patterns of PPy and PPy-*g*-MWCNT. [Color figure can be viewed in the online issue, which is available at wileyonlinelibrary.com.]

population of the C=O groups, which were only existed at the covalent junction between PPy and MWCNT, was too low to be clearly detected because of the large number of pyrrole-repeating units in PPy-*g*-MWCNT. Nevertheless, the peak shift and intensity ratio at 1567 cm^{-1} [Fig. 2(a), arrow] are an endorsing evidence for the strong interaction between PPy and MWCNT owing to the covalent links.[41]

X-ray diffraction (XRD) patterns of PPy and PPy-*g*-MWCNT are shown in Figure 2(b). The PPy shows only a broad characteristic peak centered at $2\theta = 24°$, implying that PPy is an amorphous polymer. In PPy-*g*-MWCNT, the broad characteristic peak of PPy with sharp right shoulder at $2\theta = 25.8°$ (*d*-spacing = 3.34 nm), which is corresponding to the wall-to-wall distance of MWCNT and $\pi–\pi$ stacking of PPy chains. In
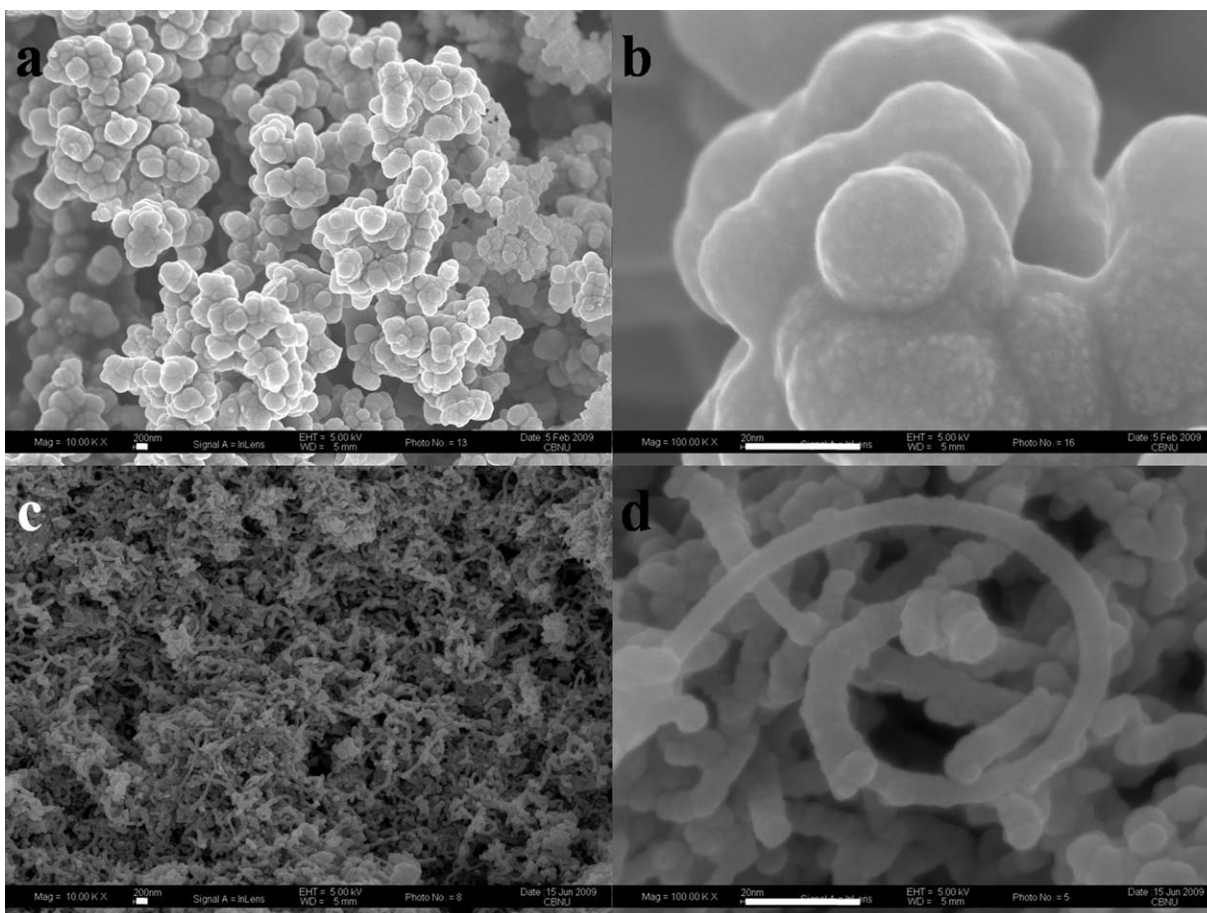

FIGURE 3 SEM images of samples: (a) PPy (×10,000); (b) PPy (×100,000); (c) PPy-*g*-MWCNT (×10,000); (d) PPy-*g*-MWCNT (×100,000). Scale bars are 200 nm.
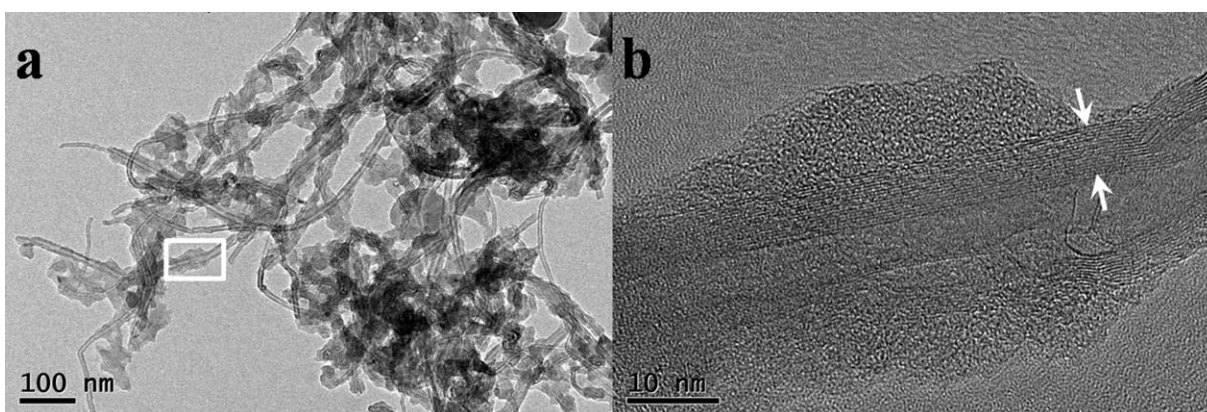
FIGURE 4 TEM images of PPy-*g*-MWCNT: (a) low magnification (×25,000) and (b) high magnification (×400,000) from rectangle in (a).

addition, full width at half maximum (FWHM) of PPy-*g*-MWCNT (10.1°) was lower than that of PPy (11.5°). This signified that the crystallinity of PPy-*g*-MWCNT was noticeably increased. It was probably because covalently linked MWCNT provided nucleation sites for PPy crystallization.

Figure 3 shows SEM images of PPy and PPy-*g*-MWCNT. The PPy displays spherical nanoscale particles with average diameter in the range of 40–400 nm [Fig. 3(a)], which is consistent with previous observations reported.[42,5] At higher magnification, the SEM image shows some protrusions that could be taken as signs of nanosized crystals on the surface [Fig. 3(b)]. In PPy-*g*-MWCNT [Fig. 3(c)], the average diameter is in the range of 40–80 nm, whose value is much larger than pristine MWCNTs (10–20 nm) and AF-MWCNTs (20–30 nm).[33] Besides, PPy-*g*-MWCNT shows rough surface with "knobby-pipe"-like morphology [Fig. 3(d)]. It is quite different from pristine MWCNTs and AF-MWCNTs [Fig. 3(c,d)]. More importantly, it is hard to observe freestanding PPy. Although noncovalent PPy wrapping could not be completely excluded, it could be an implication that PPy was most probably covalently grafted onto the surface of AF-MWCNT.

To further visually assure the covalent grafting, PPy-*g*-MWCNT was dispersed in N-methyl-2-pyrrolidone (NMP). A carbon-coated copper grid was dipped into the solution and taken out to dry in a vacuum oven. The TEM image shows that the PPy was heavily decorated onto the surface of AF-MWCNT [Fig. 4(a)]. Furthermore, the image at high magnifi-cation shows clear stripes [Fig. 4(b), arrows], which correspond to graphitic layers of MWCNTs, indicating that interior walls have remained intact during the functionalization and grafting reactions.[21,33,43,44] Therefore, the SEM and TEM results elucidate that both the reactions were remarkably effective for the functionalization of MWCNTs and grafting of PPy onto the AF-MWCNT.

Before characterizing the samples, PPy and PPy-*g*-MWCNT were carefully dedoped by immersing into 1 M aqueous NH_4OH solution, Soxhlet extracted with water, and freeze-dried under reduced pressure (0.05 mmHg) to remove the persisting presence of HCl. The sample powers were further degassed under reduced pressure (0.05 mmHg) at 100 °C. These treatments could completely eliminate HCl. The dedoped PPy and PPy-*g*-MWCNT displayed that the temperature at which 5% weight loss ($T_{d5\%}$) in air occurred at 282 and 290 °C, respectively (Supporting Information Fig. S3). The char yields of those in air at 800 °C were almost 0% for both samples. The thermo-oxidative stability of PPy-*g*-MWCNT was ~8 °C higher than that of PPy. However, it is apparent that the thermo-oxidative stability of MWCNT in PPy-*g*-MWCNT is adversely affected by the presence of PPy, whose resistance to thermo-oxidative degradation is rather poor.

UV–vis absorption and emission measurements were used to characterize the interfacial interaction between PPy and MWCNTs. Stock solutions (10.0 mg/L) were prepared by
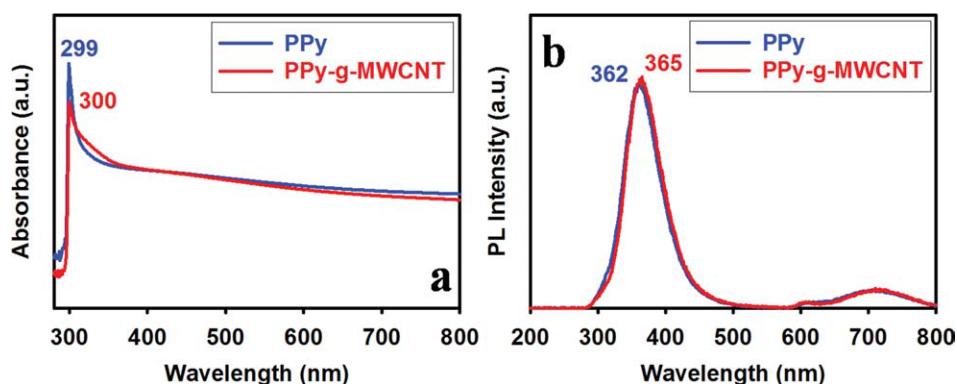

FIGURE 5 UV–vis absorption and emission spectra of sample solutions in *m*-cresol: (a) UV–vis absorption and (b) emission. [Color figure can be viewed in the online issue, which is available at wileyonlinelibrary.com.]

TABLE 1 Conductivities, BET Surface Areas, Pore Volumes, and Pore Sizes of Samples

Sample	Conductivity (S/cm)	Surface Area (m²/g)	Pore Volume (mL/g)	Pore Size (Å)
PPy	1.3×10^{-7}	76.85	0.015833	55.89
PPy-g-MWCNT	2.5×10^{-6}	52.08	0.008157	82.12

dissolving samples in m-cresol. The UV absorption spectra of PPy and PPy-g-MWCNT solutions were almost identical with sharp peaks at 299 and 300 nm, respectively [Fig. 5(a)]. The result suggested that PPy was covalently decorated on the surface of AF-MWCNT. The broad absorption band ranging from UV to near IR region implicates that both samples are dispersed well in the solvent. Fluorescent measurements of the samples were also conducted with the excitation wavelength at 300 nm, which is near the absorption maximum of PPy-g-MWCNT. The emission maxima of PPy and PPy-g-MWCNT were also similar at 362 and 365 nm, respectively [Fig. 5(b)]. Because CNTs are well known to be strong excimer quenchers and light absorbers,[45] the result further suggested that PPy was probably covalently and uniformly covering the surface of AF-MWCNT. As a result, the influence of MWCNT at excited state could almost be suppressed by the uniform decoration of PPy. If PPy-g-MWCNT was a physical mixture of PPy and AF-MWCNT by intermolecular π–π interaction in solid state, they should be segregated in solution. Thus, the peak location and emission intensity of PPy-g-MWCNT should be significantly shifted and much weakened, respectively.

Having compression-molded the samples into pellets under 60 MPa, the sheet resistances of dedoped PPy and PPy-g-MWCNT were measured by four-point probe method at room temperature. The resistance properties were measured at 10 different spots of each pellet and converted into average conductivities by the following equation $\sigma = 1/(\rho \times cf \times d)$, where σ, ρ, cf (4.4364), and d are the conductivity, the resistivity, correction factor, and sample thickness, respectively.[46] The values are summarized in Table 1. Typically, almost all conducting polymers are insulators without chemical doping. The average conductivities of dedoped PPy and PPy-g-MWCNT in this work were 1.3×10^{-7} and 2.5×10^{-6} S/cm, respectively. The conductivity of PPy-g-MWCNT was ~20 times better than that of PPy. Thus, it can be concluded that covalently linked MWCNT as conducting bridge profoundly contributed to the enhancing conductivity of PPy. The improved conductivity could be originated from an efficient charge transfer between PPy and MWCNT. PPy is an electron-rich component serving as electron-donor, whereas MWCNT is an electron-acceptor.[47] Nevertheless, the overall conductivity of PPy-g-MWCNT was not as high as would be
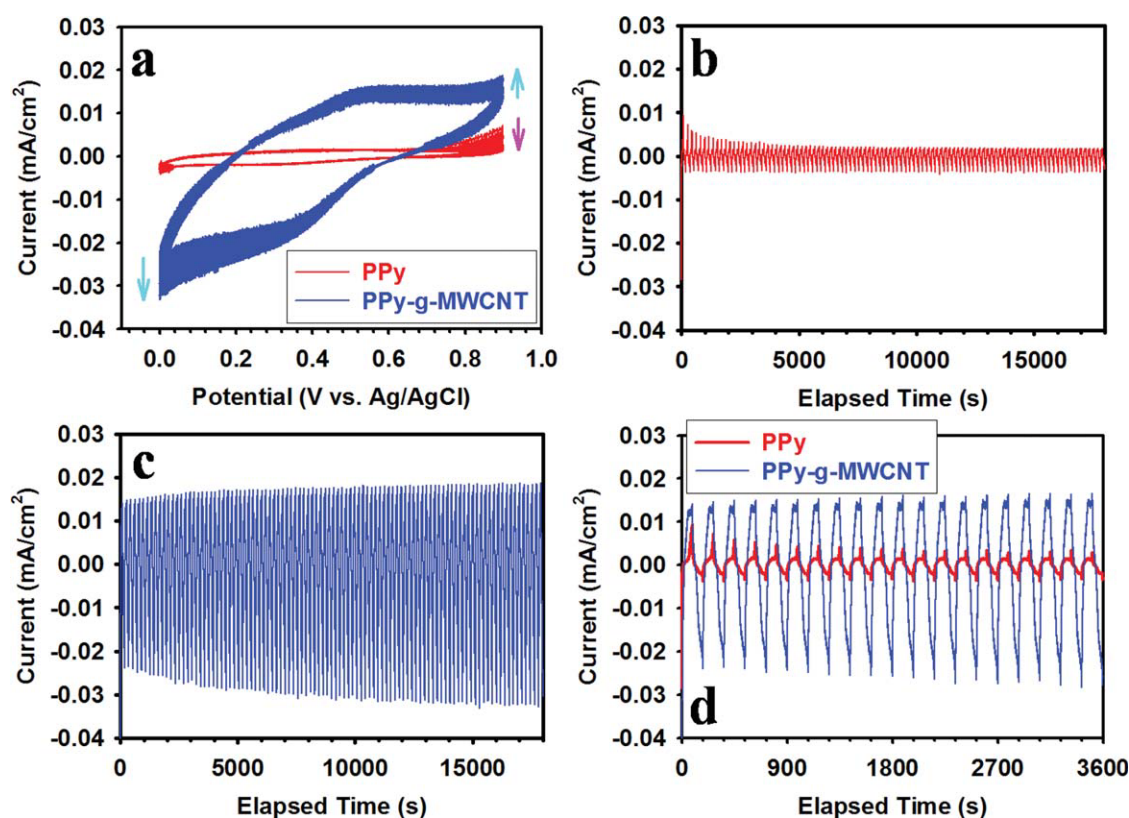

FIGURE 6 (a) Cyclic voltammograms of PPy and PPy-g-MWCNT in 0.1 M aqueous H_2SO_4 solutions. Scan rate is 10 mV/s; (b) current density changes of PPy with respect to cycle numbers; (c) current density changes of PPy-g-MWCNT with respect to cycle numbers; (d) current density changes of samples for first 20 cycles, showing cycling current stability of PPy-g-MWCNT.
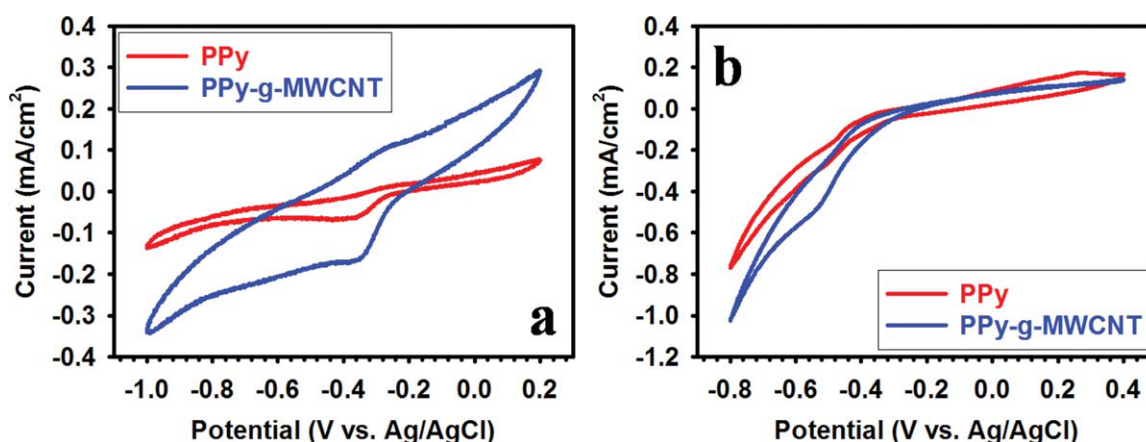
FIGURE 7 CV curves of PPy and PPy-*g*-MWCNT on GC electrodes with a scan rate of 10 mV/s: (a) in an O_2-saturated 0.1 M aqueous KOH solution and (b) in an O_2-saturated 0.1 M aqueous H_2SO_4 solution. [Color figure can be viewed in the online issue, which is available at wileyonlinelibrary.com.]

expected because the MWCNT was heavily and uniformly decorated with insulating dedoped PPy. The contact resistance must be dramatically increased by uniform PPy coats [see Fig. 3(c)]. On the basis of our previous studies,[21,38] it could be reconfirmed that MWCNT could keep their excellent properties such as conductivity during functionalization process of MWCNTs and grafting-polymerization and thus, the two-step reaction is indeed useful for the hybridization of MWCNTs and conductive polymers to expect synergetic enhancement.

The electrochemical behaviors of PPy and PPy-*g*-MWCNT were studied by using CV. The sample/GC electrodes were subjected to CV measurements using a three-electrode electrochemical cell. The test samples were prepared by evaporation of sample solution in *m*-cresol on the surface of the GC as the working electrode. The CV experiment was carried out in 0.1 M aqueous H_2SO_4 solution with a scan rate of 10 mV/s between 0 and 0.9 V. Compared with the CV curves of PPy homopolymer, those of PPy-*g*-MWCNT up to 100th cycle show profoundly high-current density [Fig. 6(a)]. It is interesting to note that the current density of PPy-*g*-MWCNT is increased as cycle number increased (sky blue arrows),

whereas the current density of PPy is drastically decreased in the beginning (pink arrow). Current–time (*I–t*) curves apparently show the current density decay in PPy [Fig. 6(b)] and amplification in PPy-*g*-MWCNT [Fig. 6(c)] with respect to cycle times. The difference between PPy and PPy-*g*-MWCNT is clearer by direct comparison of initial 20 cycles [Fig. 6(d)]. A gradual increase in current density of PPy-*g*-MWCNT should be closely related to the core–shell morphology [see Fig. 3(d)]. PPy coat on MWCNT is hygroscopic and swells as the elapsed time increased, resulting in a more efficient ion-inclusion and exclusion is possible in the shell, so as a more effective electron transport along the surface of MWCNT core.

After confirming the structure and superior electrochemical performance, PPy-*g*-MWCNT was subjected to its electrocatalytic activity for ORR. Recently, nitrogen-containing carbon materials, such as N-doped carbon nanotube (N-CNT)[34] and N-doped graphene (N-graphene),[35] are very efficient metal-free catalyst for ORR in fuel cell. Although PPy contains the nitrogen atom at every repeating unit, dedoped form is insulating material and thus, it is expected to have poor electron transport property. To show enhanced electrocatalytic
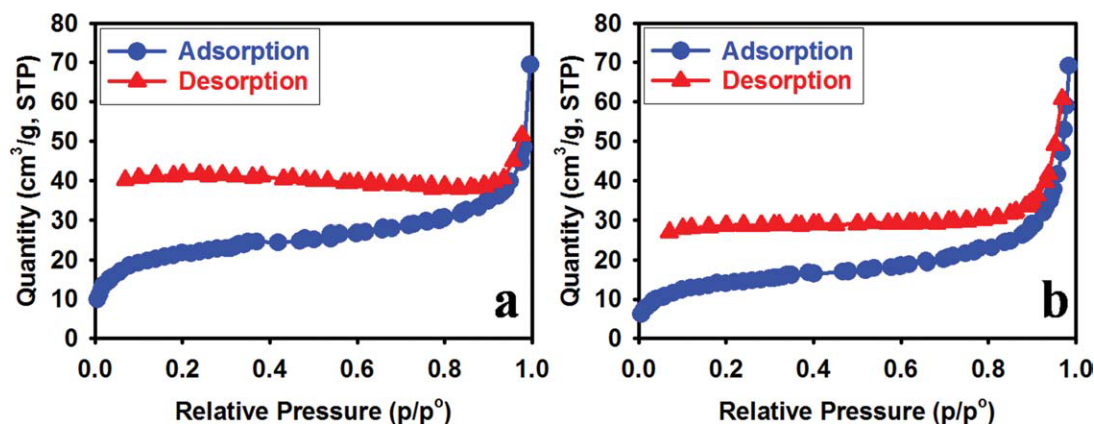

FIGURE 8 Physical adsorption and desorption isotherms of samples: (a) PPy and (b) PPy-*g*-MWCNT. [Color figure can be viewed in the online issue, which is available at wileyonlinelibrary.com.]

activity for ORR, nitrogen doping level and electrical conductivity are important factors. Thus, PPy-*g*-MWCNT satisfies the requirements and is expected to display good ORR behaviors. For the measurements of the ORR activities, sample/GC electrodes were subjected to CV measurements in an O_2-saturated 0.1 M aqueous KOH and H_2SO_4 electrolyte solutions in the potential ranges −1.0–0.2 V and −0.8–0.4 V, respectively, versus Ag/AgCl, using a sweep rate of 10 mV/s. After cycle stabilization, the 20th CV curves recorded for PPy and PPy-*g*-MWCNT coated on GC electrodes are shown in Figure 7. Although the PPy showed a negligible oxidation peak occurring at 0.3 V and a small reduction peak occurring at 0.4 V, the PPy-*g*-MWCNT showed distinct oxidation and reduction peaks occurring at the similar potentials [Fig. 7(a)], illustrating that the PPy-*g*-MWCNT electrode possessed a much higher electrocatalytic activity for ORR in basic medium. In acidic medium, both sample electrodes display featureless ORR behaviors in the potential range of −0.4 to +0.4 V [Fig. 7(b)]. The superb electrocatalytic activity of PPy-*g*-MWCNT in basic medium should be originated from the presence of acidic protons on pyrrole units in PPy, which play as charge carriers. Furthermore, covalently linking electron-rich PPy (push) and electron-poor MWCNT (full) efficiently help electron transport to enhance ORR.

The higher electroactive surface area of CNT-based nanomaterials always shows a higher electrocatalytic activity.[48–50] The specific BET surface areas of PPy and PPy-*g*-MWCNT were 76.85 and 52.08 m^2/g, respectively (Fig. 8 and Table 1). The BET surface area of PPy-*g*-MWCNT was decreased by about 32% compared with PPy homopolymer. The reduced surface area of PPy-*g*-MWCNT could be stemmed from the fact that the average diameter [see Fig. 3(d)] and crystallinity [see Fig. 2(b)] of PPy-*g*-MWCNT were increased because of uniform grafting of PPy onto the surface of AF-MWCNT and imparting it a good nucleating capability. Nevertheless, much higher electrocatalytic activity of PPy-*g*-MWCNT could be originated from the effective ion-inclusion and exclusion, and electron transport in PPy-*g*-MWCNT.

CONCLUSIONS

Given the possible presence of noncovalent polymer wrapping, PPy grafted onto 4-aminobenzoyl-functionalized MWCNT (PPy-*g*-MWCNT) composite could be prepared by a two-step reaction sequence described in this work. The composite was characterized with various analytical techniques such as FTIR, WAXD, SEM, TEM, TGA, UV–vis, and fluorescence spectroscopy. From the CV and conductivity measurement, the PPy-*g*-MWCNT nanocomposite displayed much improved electrochemical performance compared with PPy. The PPy-*g*-MWCNT also showed higher electrocatalytic activity for ORR than PPy in basic media. This result suggests that PPy-*g*-MWCNT can be very useful catalyst for fuel cell applications. This work illustrates that a two-step reaction sequence involving Friedel–Crafts functionalization and the subsequent grafting is indeed a useful approach for the hybridization of carbon-based nanomaterials and functional polymers toward multifunctional/materials systems.

REFERENCES AND NOTES

1 Chen, Y.-S.; Li, Y.; Wang, H.-C.; Yang, M.-J. Carbon 2007, 45, 357–363.

2 Jurewicz, K.; Delpeux, S.; Bertagna, V.; Béguin, F.; Frackowiak, E. Chem Phys Lett 2001, 347, 36–40.

3 Wu, T.-M.; Yen, S.-J.; Chen, E.-C.; Chiang, R.-K. J Polym Sci Part B: Polym Phys 2008, 46, 727–733.

4 Wu, T.-M.; Lin, S.-H. J Polym Sci Part B: Polym Phys 2006, 44, 1413–1418.

5 Fan, J.; Wan, M.; Zhu, D.; Chang, B.; Pan, Z.; Xie, S. J Appl Polym Sci 1999, 74, 2605–2610.

6 Gangopadhyay, R.; De, A. Chem Mater 2000, 12, 608–622.

7 Sonoda, Y.; Takashima, W.; Kaneto, K. Synth Met 2001, 119, 267–268.

8 Sahoo, N. G.; Jung, Y. C.; Goo, N. S.; Cho, J. W. Macromol Mater Eng 2005, 290, 1049–1055.

9 Xian, Q.; Zhou, X. Electrochim Acta 2003, 48, 575–580.

10 Little, S.; Ralph, S. F.; Too, C. O.; Wallace, G. G. Synth Met 2009, 159, 1950–1955.

11 Kim, J. S.; Kim, W. J.; Cho, N.; Shukla, S.; Yoon, H.; Jang, J.; Prasad, P. N.; Kim, T.-D.; Lee, K.-S. J Nanosci Nanotechnol 2009, 9, 6957–6961.

12 Huang, W. S.; Humphrey, B. D.; MacDiarmid, A. G. J Chem Soc Faraday Trans 1986, 82, 2385–2400.

13 Saunders, B. R.; Fleming, R. J.; Murray, K. S. Chem Mater 1995, 7, 1082–1094.

14 Waller, A. M.; Hampton, A. N. S.; Compton, R. G. J Chem Soc Faraday Trans 1989, 85, 773–781.

15 Thostenson, E. T.; Ren, Z.; Chou, T.-W. Compos Sci. Technol 2001, 61, 1899–1912.

16 Gooding, J. J. Electrochim Acta 2005, 50, 3049–3060.

17 Schadler, L. S.; Giannaris, S. C.; Ajayan, P. M. Appl Phys Lett 1998, 73, 3842–3844.

18 Qian, D.; Dickey, E. C.; Andrews, R.; Rantell, T. Appl Phys Lett 2000, 76, 2868–2870.

19 Biughman, R. H.; Zakhidov, A. A.; de Heer, W. A. Science 2002, 297, 787–792.

20 Dai, L.; Mau, A. W. H. Adv Mater 2001, 13, 899–913.

21 Jeon, I.-Y.; Lee, H.-J.; Choi, Y. S.; Tan, L.-S.; Baek, J. B. Macromolecules 2008, 41, 7423–7432.

22 Dong, B.; He, B.-L.; Xu, C.-L.; Li, H.-L. Mater Sci Eng B 2007, 143, 7–13.

23 Ago, H.; Petritsch, K.; Shaffer, M. S. P.; Windle, A. H.; Friend R. H. Adv Mater 1999, 11, 1281–1285.

24 Hughes, M.; Chen, G. Z.; Shaffer, M. S.; Fray, D. J.; Windle, A. H. Chem Mater 2002, 14, 1610–1613.

25 Chen, J.; Rao, A. M.; Lyuksyutov, S.; Itkis, M. E.; Hamon, M. A.; Hu, H.; Cohn, R. W.; Eklund, P. C.; Colbert, D. T.; Smalley, R. E.; Haddon R. C. J Phys Chem B 2001, 105, 2525–2528.

26 Ramesh, A.; Ericson, L. M.; Davis, V. A.; Saini, R. K.; Kittrell, C.; Pasquali, M.; Billups, W. E.; Adams, W. W.; Hauge, R. H.; Smalley, R. E. J Phys Chem B 2004, 108, 8794–8798.

27 Monthioux, M.; Smith, B. W.; Burteaux, B.; Claye, A.; Fischer, J. E.; Luzzi, D. E. Carbon 2001, 39, 1251–1272.

28 Zhang, Y.; Shi, Z.; Gu, Z.; Iijima, S. Carbon 2008, 38, 2055–2059.

29 Salzmann, C. G.; Llewellyn, S. A.; Tobias, G.; Ward, M. A. H.; Huh, Y.; Green, M. L. H. Adv Mater 2007, 19, 883–887.

30 Heller, D. A.; Barone, P. W.; Strano, M. S. Carbon 2005, 43, 651–653.

31 Sammalkorpi, M.; Krasheninnikov, A.; Kuronen, A.; Nordlund, K.; Kaski, K. Phys Rev B 2004, 70, 245416-1–245416-8.

32 Baek, J.-B.; Lyon, C. B.; Tan, L.-S. J Mater Chem 2004, 14, 2052–2056.

33 Lee, H.-J.; Han, S.-W.; Kwon, Y.-D.; Tan, L.-S.; Baek, J.-B. Carbon 2008, 46, 1850–1859.

34 Gong, K. P.; Du, F.; Xia, Z. H.; Dustock, M.; Dai, L. M. Science 2009, 323, 760–764.

35 Qu, L. T.; Liu, Y.; Baek, J.-B.; Dai, L. M. ACS Nano 2010, 4, 1321–1326.

36 http://www.hanwhananotech.co.kr. Accessed on April 4, 2011.

37 Baek, J.-B.; Tan, L.-S. Polymer 2003, 44, 4135–4147.

38 Jeon, I.-Y.; Tan, L.-S.; Baek, J.-B. J Polym Sci Part A: Polym Chem 2010, 48, 1962–1972.

39 Song, Y. S.; Youn, J. R. Carbon 2005, 43, 1378–1385.

40 Ajayan, P. M.; Schadler, L. S.; Giannaris, C.; Rubio, A. Adv Mater 2000, 12, 750–753.

41 Milena, G.-M.; Janis, G. M.; Raoul, C.; George, P. S.; Peter, M. F. Chem Mater 2006, 18, 6258–6265.

42 Shen, Y. Q.; Wan, M. X. J Appl Polym Sci 1998, 68, 1277–1284.

43 Jeon, I.-Y.; Tan, L.-S.; Baek, J.-B. J Polym Sci Part A: Polym Chem 2008, 46, 3471–3481.

44 Han, S.-W.; Oh, S.-J.; Tan, L.-S.; Baek, J.-B. Carbon 2008, 46, 1841–1849.

45 Guo, M.; Chen, J.; Li, J.; Tao, B.; Yao, S. Anal Chim Acta 2005, 532, 71–77.

46 Perloff, D. S. Solid State Electron 1977, 20, 681–687.

47 Wu, T.-M.; Lin, Y.-W.; Liao, C.-S. Carbon 2005, 43, 734–740.

48 Laviron, E. J Electroanal Chem 1979, 100, 263–270.

49 Laviron, E. J Electroanal Chem 1979, 101, 19–28.

50 Winter, M.; Brodd, R. J. Chem Rev 2004, 104, 4245–4269.